buildings

MDPI

Article

Assessment of Reinforcement Steel–Concrete Interface Contact in Pullout and Beam Bending Tests Using Test-Fitted Cohesive Zone Parameters

Paulo Fernando Matos Santana, Francisco Evangelista Junior * and Marcos Honorato Oliveira

Graduate Program in Structures and Civil Construction—PECC, Department of Civil and Environmental Engineering—ENC, Faculty of Technology, University of Brasilia, Brasilia 70910-900, Brazil; santana.paulo@aluno.unb.br (P.F.M.S.)
* Correspondence: fejr@unb.br

Abstract: Modeling the steel-concrete interface is a constant research topic in structural engineering. Several studies have explored advanced modeling methods, including cohesive models. This article fits into this context by investigating the bond strength at the steel-concrete interface based on a cohesive model. The numerical parameters considered in the software ABAQUS 2019 are investigated. The experimental and numerical results of pullout and beam tests were used as references for the parameters fitting process. With the Concrete Damaged Plasticity model (CDP), the physical nonlinearity of the concrete was considered. The contact was described as a surface-to-surface interaction. The pullout tests' cohesive parameters were fitted with experimental tests. Regarding the beam models, an analysis was carried out verifying the use of pullout fitting parameters in the beam models, aiming to compensate for the eventual absence of these data. For the pullout models, the cohesive parameters fitting process yielded better results than those obtained with the recommended values. Improvements were especially significant regarding slippage at the maximum pullout force. The use of pullout test-fitted parameters in the beam models had a smaller influence on the ultimate load predictions. However, the slippage predictions and beam deflection were more affected by the change in cohesive parameters. The bond modeling using a surface-based technique performed well at a low computational cost, considering the materials' physical nonlinearities and 3D geometries. The results, also in general, did not significantly change the load predictions, which indicates a possibility of use in numerical simulations when the pullout data is available.

Keywords: steel–concrete interface; contact; cohesive model; concrete damaged plasticity

check for updates

Citation: Santana, P.F.M.; Evangelista Junior, F.; Oliveira, M.H. Assessment of Reinforcement Steel–Concrete Interface Contact in Pullout and Beam Bending Tests Using Test-Fitted Cohesive Zone Parameters. *Buildings* **2024**, *14*, 2981. https://doi.org/10.3390/buildings14092981

Academic Editor: Vipul Patel

Received: 28 May 2024
Revised: 19 June 2024
Accepted: 28 June 2024
Published: 20 September 2024

Copyright: © 2024 by the authors. Licensee MDPI, Basel, Switzerland. This article is an open access article distributed under the terms and conditions of the Creative Commons Attribution (CC BY) license (https://creativecommons.org/licenses/by/4.0/).

1. Introduction

Motivated by the large-scale applications of reinforced concrete in civil construction in recent decades, scientific advances in structural engineering have contributed to the development of analytical methods that aim to better understand the behavior of this material. Theoretical and experimental research were crucial elements in achieving this goal. However, the experimental investigation of different structure types and physical phenomena often becomes restricted due to the physical and economic aspects inherent to the experimental tests and the analysis's complexity. As mentioned by Wolensky et al. [1], factors related to reinforced concrete, such as cracking, crushing, creep, reinforcement yielding, and bond failure, among other phenomena, contribute to the experimental campaign limitations.

In this context, the computational modeling of reinforced concrete structures has taken advantage of the increasing progress of computational mechanics in such a way that these and other complex phenomena can be modeled in a reasonably realistic way. One of the most widespread numerical methods in structural analysis is the finite element method

(FEM), which allows complex simulations of reinforced concrete structures, including the contact interaction of different nonlinear materials.

According to [2], the bond between rebar and the concrete matrix is one of the major factors that affect the mechanical behavior of this composite material. Knowing the parameters that influence the behavior of the steel-concrete interface becomes fundamental for the development of analytical models for the bond stress as a function of the interface slip [3].

As demonstrated in [4,5], the bond strength at the steel-concrete interface is one of the most difficult problems to face in the study of reinforced concrete, and researchers still do not completely understand its behavior. It occurs due to the great number of parameters needed to represent the bond phenomena, making the study of bond behavior very important.

The first studies related to the bond of steel bars embedded in concrete appeared at the end of the 19th century, with the first scientific papers published at the beginning of the 20th century, according to [6,7]. After a few years, in the 1970s, 80s, and 90s, experimental investigations explored various aspects of the subject, constituting the basis for the development of current calculation methods. In the last 20 years, numerical studies were carried out to expand the knowledge about the pullout of steel bars, bond mechanisms, and the global behavior of structural elements in reinforced concrete considering the bond loss at the steel-concrete interface [8].

Currently, the usual way to measure contact behavior has been through the definition of bond stress. The stress distribution along the steel-concrete interface has great relevance in the load capacity and service status of reinforced concrete parts. It is well-known in the literature that the stress transfer mechanism between steel and concrete can be defined in three stages: chemical adhesion, friction, and mechanical action. In smooth bars, bar pullout is predominantly caused by the failure of the chemical adhesion between the cement paste and the bar. When chemical adhesion is broken, resistance due to friction arises. In ribbed bars, the slip resistance is mainly due to the mechanical action between the concrete and the ribs. Also, factors that influence the bond strength and the failure mode of the reinforced concrete parts are the quality of the cement paste used in the mixture, the rebar surface roughness, concrete covering, steel yield strength, diameter, spacing, and the location of the bar in the concrete cross-section and adequate confinement level of the tensioned bars. According to [9], the concrete confinement level is achieved by the stirrups that absorb part of the stresses from the radial splitting that occurs between the steel bar under tension and the adjacent concrete.

One method to simulate the bond mechanism of steel bars embedded in concrete is the cohesive zone model (CZM). This model is capable of simulating fracture (or surface) separation as a gradual phenomenon across an extended crack tip, or cohesive zone, and is resisted by cohesive tractions to physically represent nonlinear processes located at the crack front or surface separation zones [10,11]. The CZM has been widely used in the literature to model a variety of problems showing its versatility and efficiency [12–15], also including applications to the rebar–concrete interface [16–19].

Considering the aforementioned context, the main objective of this paper is to evaluate the influence of the numerical parameters considered with the finite element commercial software ABAQUS 2019 in the bond-slip modeling in the steel-concrete interface contact based on the cohesive zone model. The physical non-linearity of the concrete was considered by the Concrete Damaged Plasticity model (CDP) available in the software. The computational modeling is carried out for the two types of known experiments in the bond-slip relationship study: pullout and beam tests. The results provided by the numerical analysis were fitted and compared to the numerical–experimental research carried out by Almeida Filho [20], with pullout and beam tests following the RILEM-FIP-CEB recommendations [21,22]. The main contribution is the quantitative assessment of the validity and accuracy of using the recommended values for cohesive properties obtained for pullout tests. This paper addresses whether those recommendations are valid and lead to satisfactory results for modeling pullout and beam tests when compared to test-fitted

properties' values customized to each test. Furthermore, no paper in the literature quantitatively addresses those questions, especially using cohesive zone models, whose fitted properties are constantly questioned in the literature.

2. Background in Bond Slip

The steel-concrete interface modeling can be interpreted in two ways. In numerical analyses of real-scaled reinforced concrete structures, the steel bars are generally modeled as beam or truss elements. In this case, a perfect bond to the concrete is assumed, with satisfactory results. However, if a local analysis of the steel-concrete bond is performed, the perfect bond simplification may not provide a real picture of bond behavior, requiring the modeling of bond properties as a function of relative slip [23].

In cases where a perfect bond is adopted, the spring model is one of the simplest to represent such behavior. This model can be understood as two orthogonal springs that connect the nodes of the two materials in a way that appropriate stress-strain relationships eliminate any relative displacement between them, implying a simultaneous identity and the same degrees of freedom [24,25]. In the software ABAQUS, a spring-translator element is available to simulate the bond-slip phenomena in reinforced concrete during pullout tests [26].

Also, a perfect bond can be achieved with the embedded region technique to simulate steel bars embedded in solid concrete elements, as shown in Figure 1a. The program looks for the geometric relationships between the nodes of the embedded elements and the elements of the host material. If a node of an embedded element is inside a host element, the translational degrees of freedom in the node are eliminated, and the node becomes an "embedded node". Thus, the translational degree of freedom of the embedded node is constrained to the interpolated values of the degree of freedom corresponding to the host element [27].

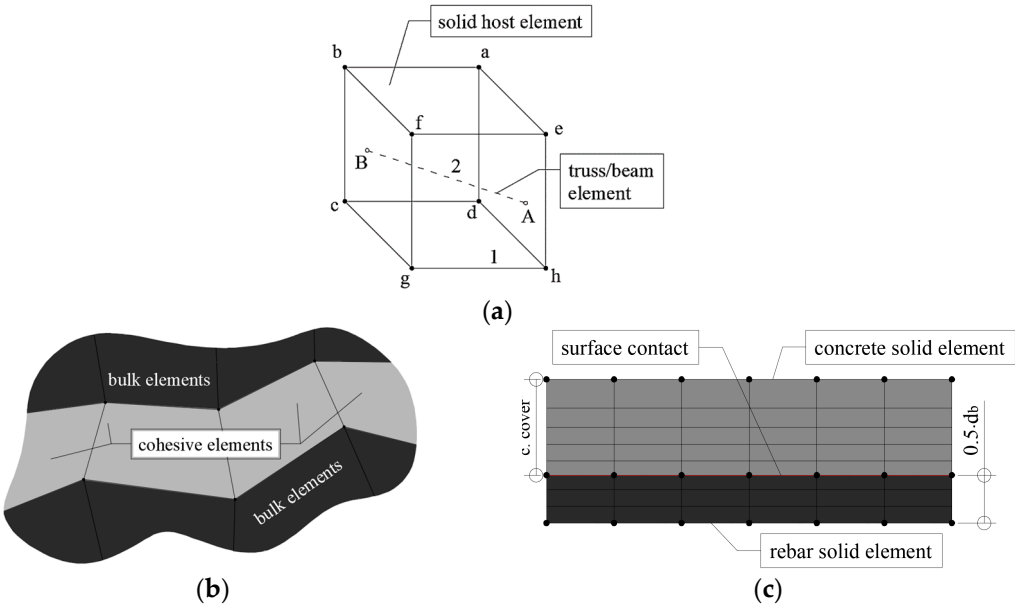


Figure 1. Modeling strategies for the steel-concrete interface: (**a**) perfect bond (embedded region); (**b**) contact elements; (**c**) surface contact.

The steel-concrete interface modeling uses the concepts of cohesive zone models and can be separated basically into two strategies [28] and two levels of detail [8]. Strategies differ in using contact elements and contact surfaces, as shown in Figure 1b,c. The detail levels differ in the detailed modeling, where the bar ribs can be discretized or simplified, in a phenomenological modeling way. Some numerical modeling applications using the CZM concepts, nonlinear damage constitutive models for concrete, and surface-based

techniques in reinforced concrete structures and other materials, with different applications, are presented in [12–19,29–38].

Brisotto [39] establishes that the bond mechanisms that govern the model of smooth bars are the same as those of ribbed bars but in different intensities. For the ribbed bars, the chemical adhesion contribution is very small, while in smooth bars, the ability to generate normal stresses is much lower due to the low roughness and the absence of protrusions such as ribs.

According to Pereira et al. [8], the detailed discretization of the ribs demands a high computational cost due to mesh refinement. Therefore, smooth bar simplification is normally adopted in cases of three-dimensional analysis. In this case, the connection of the elements can be made through a discontinuous approach where a discrete bond zone is modeled with elements of reduced thickness and controlled by an appropriate bond–slip stress relationship. Beliaev et al. [40] concluded that models with a perfect bond could not predict the maximum bond stress, not even the post-peak. The authors also observed no significant differences between the elastoplastic and the elastoplastic with damage constitutive model for the concrete, and both are more efficient than the linear elastic model.

Thus, as mentioned before, in the ABAQUS software, the cohesive behavior can be represented by a contact element approach (element-based), surface contact approach (surface-based), and user-defined elements through Python scripts [27]. In the contact element approach, the definition of a linear elastic material with damage is required, and a traction–separation law is applied to this material. In the surface-based approach, there is no need to create new material and therefore, the cohesive properties are attributed to the surfaces in contact. The cohesive behavior is represented by the definition of the linear elastic portion, damage initiation criterion, and damage evolution law. Linear elastic behavior is written in terms of an elastic constitutive matrix, as shown in Equation (1) [27].

$$\boldsymbol{t} = \begin{Bmatrix} t_n \\ t_s \\ t_t \end{Bmatrix} = \begin{bmatrix} K_{nn} & K_{ns} & K_{nt} \\ K_{ns} & K_{ss} & K_{st} \\ K_{nt} & K_{st} & K_{tt} \end{bmatrix} \begin{Bmatrix} \delta_n \\ \delta_s \\ \delta_t \end{Bmatrix} = \boldsymbol{K\delta} \tag{1}$$

where t_n, t_s, and t_t are the normal and shear stresses, K_{nn}, K_{ss}, and K_{tt} are the penalty contact parameters in the normal and shear directions, and δ_n, δ_s, and δ_t are the normal and shear separations, respectively. A simplified approximation for the contact penalties is presented by Luna Molina et al. [41], supported by the research findings in [42,43], as shown in Equations (2) and (3). According to [44], because there is a lack of experimental research regarding the local bond stiffness between a steel bar and concrete in the direction normal to the interface, the assumption made by Keuser et al. [38] is used in this paper. The normal bond stiffness is assumed to equal 100 times the tangent bond stiffness, which is obtained by the approximation of the bond-slip relationship prescribed by the *fib* Model Code 2010 [45].

$$K_{ss} = K_{ss} = \frac{\tau_{\max}}{s_1} \tag{2}$$

$$K_{nn} = 100K_{ss} = 100K_{tt} \tag{3}$$

where τ_{max} is the maximum shear stress, and s_1 is the displacement when τ_{max} is reached. These parameters are established in the *fib* Model Code 2010 [45] bond-slip relationship, which is widely used in the validation of experimental and numerical studies of bond strength between steel and concrete, as presented in [16–19,46].

The criteria for the damage initiation are the maximum contact stress, maximum separation, or the quadratic interactions of both functions, respectively, as shown in Equations (4)–(7):

$$\max\left\{\frac{\langle t_n\rangle}{t_n^0}, \frac{\langle t_s\rangle}{t_s^0}, \frac{\langle t_t\rangle}{t_t^0}\right\} = 1 \tag{4}$$

$$\max\left\{\frac{\langle \delta_n\rangle}{\delta_n^0}, \frac{\langle \delta_s\rangle}{\delta_s^0}, \frac{\langle \delta_t\rangle}{\delta_t^0}\right\} = 1 \tag{5}$$

$$\left\{\frac{\langle t_n \rangle}{t_n^0}\right\}^2 + \left\{\frac{t_s}{t_s^0}\right\}^2 + \left\{\frac{t_t}{t_t^0}\right\}^2 = 1 \quad (6)$$

$$\left\{\frac{\langle \delta_n \rangle}{\delta_n^0}\right\}^2 + \left\{\frac{\delta_s}{\delta_s^0}\right\}^2 + \left\{\frac{\delta_t}{\delta_t^0}\right\}^2 = 1 \quad (7)$$

In damage evolution, the criterion describes the rate of material stiffness degradation once the corresponding damage initiation criteria have been reached. The stress response after damage initiation evolves according to a linear scalar damage equation where the factor $(1 - d)$ multiplies each component of contact stress that would be predicted by the linear elastic behavior of the traction–separation law in the undamaged point. The damage variable is composed of between 0 and 1. When $d = 0$ and $d = 1$ they represent the responses of the intact and entire damaged material, respectively.

The damage evolution law can be specified as effective displacement or fracture energy. In both cases, linear or exponential curves are considered, and mixed modes of damage can also be included, where the appropriate properties are specified for each direction. For damage evolution by displacement, it is necessary to define the displacement value at maximum traction. The ABAQUS user can also explicitly enter the variable d as a function of the displacement [28] in a tabular form.

3. Proposed Finite Element Modeling and Simulation

In the following subsections, the test configurations, boundary conditions, loading scheme, finite element mesh, materials properties definitions, and parameters for the cohesive and concrete constitutive model are presented.

3.1. Test Configurations

In this paper, the numerical models were based on experimental tests that study the bond behavior in pullout tests of steel rebars embedded in concrete cylinder specimens and reinforced concrete beams, following the RILEM-FIP-CEB reports [21,22].

The specimens differ by the concrete compressive strength, the rebar bonding (or contact) length, and the bar diameter. The labels for each model follow this reasoning: "A" and "V" stand for pullout models and beam models, respectively. "C30" and "C60" indicate the expected concrete compressive strength. "B10" and "B16" represent the bar diameters used. The specimen's geometries of the pullout and beam experimental tests, with dimensions in cm, are shown in Figure 2. For each pullout specimen, five tests were carried out, and for each configuration of the beam model, two repetitions were carried out.

3.2. Boundary Conditions, Loading, and Finite Element Mesh

Only ¼ of each experiment was modeled in ABAQUS to obtain a lower computational cost using the benefits of symmetry. Figure 3 shows the applied boundary conditions, where in the pullout models the upper cross-section of the steel bar was restricted to vertical displacements, and the vertical displacement that simulates the pullout force was applied to the upper face of the concrete.

In the beam models, the boundary conditions of simple support, symmetry planes, hinge, and vertical displacement that simulate the loading on the beam were applied according to the experimental setup.

For all other constructive reinforcements embedded in the concrete beam models, the "Embedded Region" constraint was applied. Thus, all the nodes of the bar elements of these reinforcements were linked to the degrees of freedom of the nearby nodes belonging to the host element, which was the concrete matrix. In the pullout models, no reinforcement was used other than the rebar used for the pullout application.

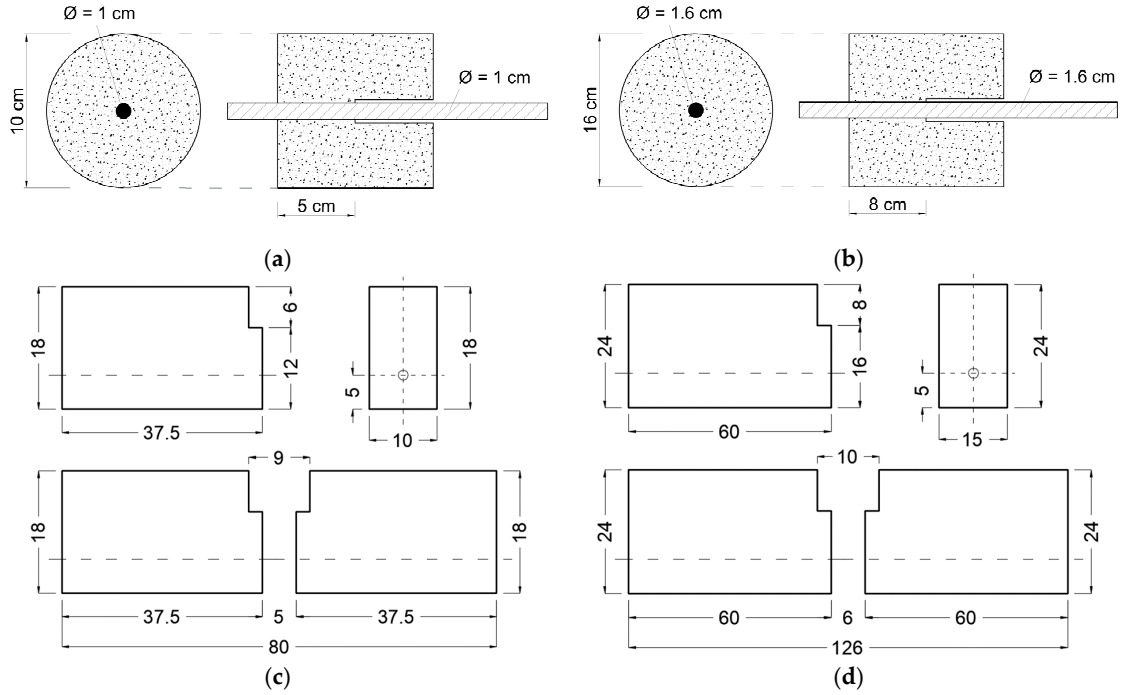


Figure 2. Models: (**a**) Pullout test with 10 mm bar; (**b**) pullout test with 16 mm bar; (**c**) beam test with 10 mm bar; (**d**) beam test with 16 mm bar (units in cm).

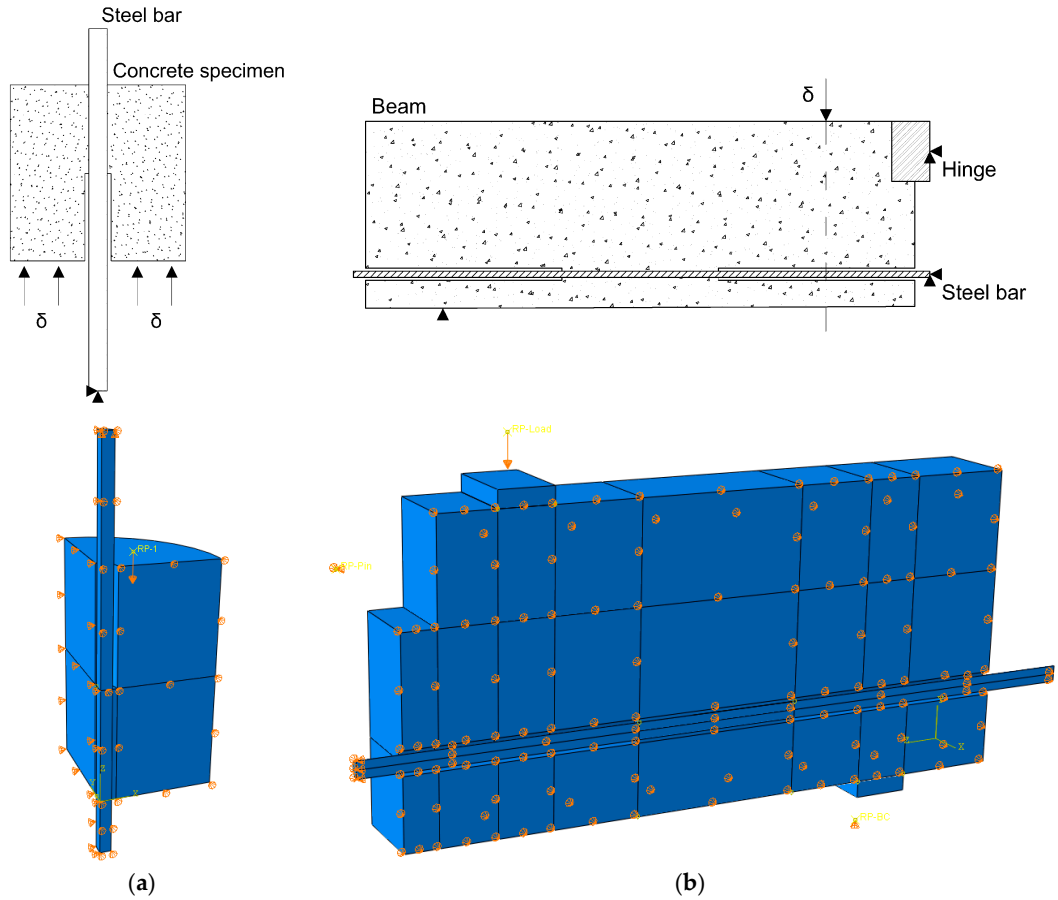
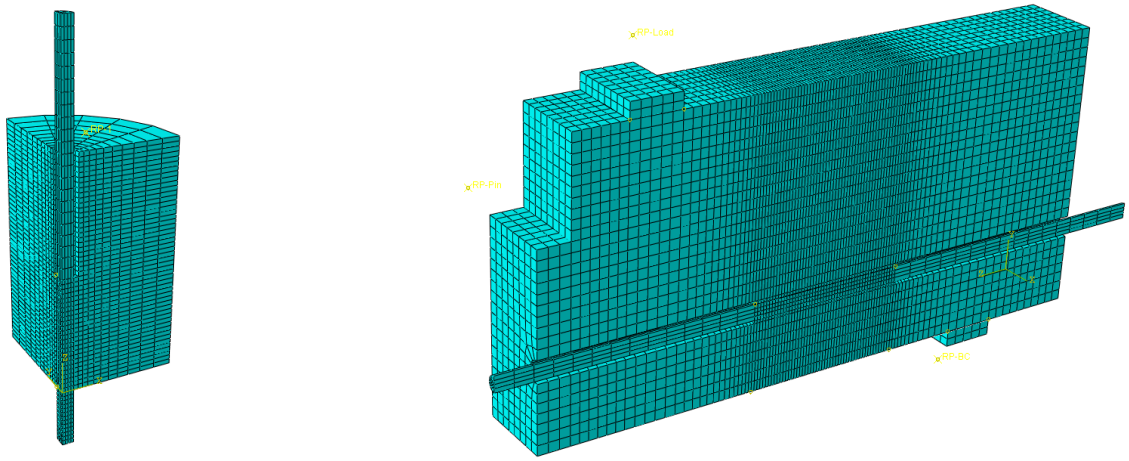


Figure 3. Idealization and boundary conditions application in the numerical models: (**a**) pullout test; (**b**) beam test.

All numerical models were discretized with an 8-node linear brick, with reduced integration and hourglass control (C3D8R). Partition planes were drawn to obtain a uniform meshing. The desired element characteristic length was 2 mm. The central part of the beam, which had the steel–concrete contact, was discretized with the fine mesh, and the rest of the beam, far away from the contact, had a 6 mm element length for the mesh, as shown in Figure 4.



(**a**) (**b**)

Figure 4. Final mesh of the models: (**a**) pullout test; (**b**) beam test.

The locations prioritized applying a more refined finite element mesh in the numerical models following the same recommendations applied in other studies [16–19]. Tests were carried out with coarser meshes, but the results were compromised due to the contact algorithm, which requires greater mesh refinement in the contact region.

In addition to the experimental tests, the numerical analysis developed in this research in the ABAQUS software was compared with the numerical modeling carried out by [20] through ANSYS v6.1 software.

3.3. Materials

The experimental tests were carried out by Almeida Filho [20]. Two experimental campaigns were performed with the expected concrete strength of 30 MPa and 60 MPa, respectively. In both series, the bars' diameters were also varied, with 10 mm and 16 mm steel bars. The main material properties used in the numerical analysis are presented in Table 1. Poisson ratios of 0.20 and 0.30 were used for concrete and steel, respectively.

Table 1. Concrete and steel material properties.

Specimen		Concrete				Steel	
	l_b (mm)	f_{cm} (MPa)	E_c (MPa)	f_{ctm} (MPa)	f_{ys} (MPa)	E_s (MPa)	Ø (mm)
A-C30-B10	50	32.02	27,237	1.96	570	207,050	10
A-C30-B16	80	32.02	27,237	1.96	630	209,180	16
A-C60-B10	50	61.00	32,614	3.10	570	207,050	10
A-C60-B16	80	61.00	32,614	3.10	630	209,180	16
V-C30-B10	50	32.02	27,237	1.96	570	207,050	10
V-C30-B16	80	32.02	27,237	1.96	630	209,180	16
V-C60-B10	50	61.00	32,614	3.10	570	207,050	10
V-C60-B16	80	61.00	32,614	3.10	630	209,180	16

3.4. Contact Interaction Properties

The surface-to-surface interaction describes the contact between steel and concrete. The interaction properties, such as normal, tangential behavior, cohesive behavior, and

damage properties of the contact, are defined for each model based on experimental results [20] used to validate the numerical models.

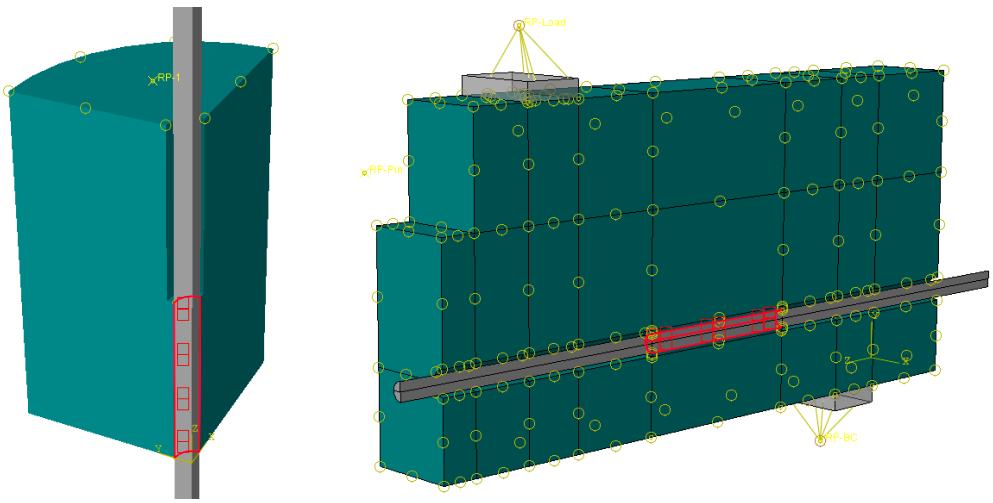
The values used in numerical simulations are shown in Table 2, particularly for the cohesive behavior, in terms of the cohesive parameters calculated from Equations (2) and (3), and the damage parameters. The damage evolution law was defined based on the known displacement at the maximum bond stress obtained experimentally. Normal and shear stress values were also obtained from experimental tests. The viscosity coefficient was set equal to 10^{-3}.

Table 2. Contact interaction properties of the numerical models.

Specimen	Cohesive Behavior		Damage Parameters		
	K_{nn} (MPa/mm)	$K_{ss} = K_{tt}$ (MPa/mm)	Normal Stress (MPa)	Shear Stress (MPa)	Plastic Displacement (mm)
A-C30-B10	1177	11.77	1.96	11.52	6.02
A-C30-B16	642	6.42	1.96	10.53	7.00
A-C60-B10	1279	12.79	3.10	15.73	1.23
A-C60-B16	1037	10.37	3.10	21.31	2.00
V-C30-B10	4519	45.19	1.96	13.33	0.29
V-C30-B16	1741	17.41	1.96	13.20	0.76
V-C60-B10	24,338	243.38	3.10	16.55	0.07
V-C60-B16	2568	25.68	3.10	16.95	0.02

The normal behavior was defined with a "hard" pressure–overclosure contact type, in all models. The tangential behavior was defined with the penalty friction formulation, with a friction coefficient equal to 0.50, which is close to the recommendation for pullout failure according to [46].

Figure 5 shows the numerical models' surfaces with applied cohesive contact properties, highlighted in red squares, and the solid elements with embedded regions are indicated with yellow circles. In all models, the master and slave surfaces were defined as steel bars and concrete, respectively. No other surfaces were given contact properties. In the regions of support and load application for the beam models, the surfaces between the concrete beam and the metallic supports were fixed through the tie-type constraint.



(**a**) (**b**)

Figure 5. Surfaces with cohesive contact properties: (**a**) pullout test; (**b**) beam test.

3.5. CDP Numerical Parameters

The Concrete Damaged Plasticity Model (CDPM) provides a general capability for modeling concrete and other quasi-brittle materials, using concepts of isotropic damaged elasticity in combination with isotropic tensile and compressive plasticity [27]. To define the CDP model, the authors used the methodology published by Alfarah et al. [47]. All the input data, such as numerical parameters, compressive and tensile behavior, and damage variable calculations, follow the recommendation of the latter cited reference. The CDP parameters used in the analysis are shown in Table 3.

Table 3. Numerical parameters of the CDP model.

ψ	ε	f_{b0}/f_{c0}	K_c	μ
13°	0.1	1.16	0.667	0.001

Where ψ is the dilation angle, ε is the flow potential eccentricity, f_{b0}/f_{c0} is the ratio of biaxial compressive yield strength and uniaxial compressive yield strength, K_c is the ratio of the second stress invariant on the tensile meridian, and μ is the viscosity parameter. The numerical parameters used in this research are based on very satisfactory results for the FE concrete modeling, as demonstrated in [18,48–55]. Other successful applications of damage models for concrete in different numerical modelings are presented in [56–59].

4. Numerical Results

This section presents the analysis outcomes of the numerical models developed using the surface-based cohesive model applied to the surface-to-surface interaction property in ABAQUS. Almeida Filho [20] conducted numerical tests with the modified Mohr-Coulomb model using the software ANSYS. For representing the experimental results, only the average curve of the results was used. For the pullout models, the specimens with 10 mm bars obtained standard deviations equal to 1.7 and 4.0 for the 30 MPa and 60 MPa concrete. The specimens with 16 mm bars obtained values equal to 1.6 and 6.5 for the 30 MPa and 60 MPa concrete. For the beam models, the same configurations of bar diameter and concrete grade obtained standard deviations equal to 2.1, 6.4, 1.1, and 6.4, respectively. Although they are different situations, the results share similarities with the results of Santana et al. [56], specially the convergence of pullout results and computational modeling based on experimental tests.

4.1. Pullout Model

The stress fields observed in the models are shown in Figure 6, in terms of von Mises stresses and principal stresses. As an effect of the mechanical adhesion provided by the ribs of the bar, compression strips propagate from the bond zone to the concrete surface, as shown in Figure 6. A system of circumferential tension cracks runs from the load transfer zone around the bonded length.

The results of the cohesive parameters fitting process were compared to the recommended values in Figure 7. Later, are presented the fitted cohesive parameters for each model in Table 4. Specimens with 30 MPa concrete had a sliding failure mode, while specimens with 60 MPa concrete had a splitting failure mode. The numerical results obtained for the models with slip failure mode were like the results found in [18].

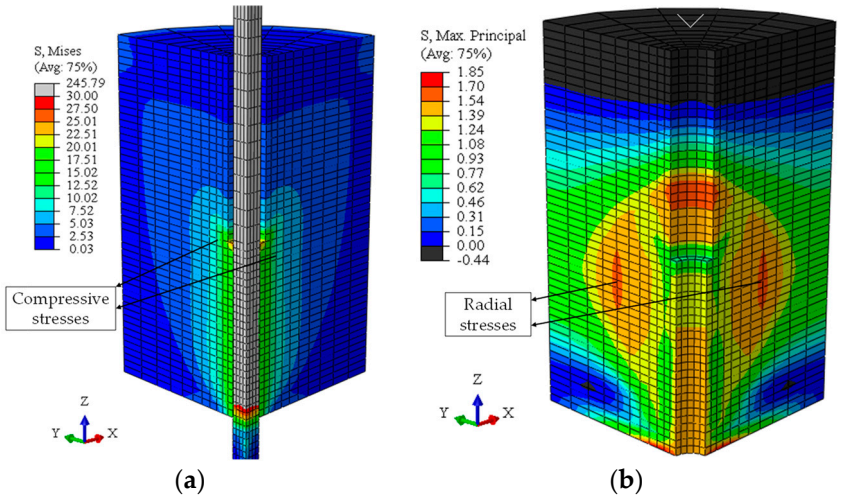


Figure 6. Stresses at the final of pullout simulation of A-C40-B10 model: (**a**) Von Mises; (**b**) Maximum Principal.

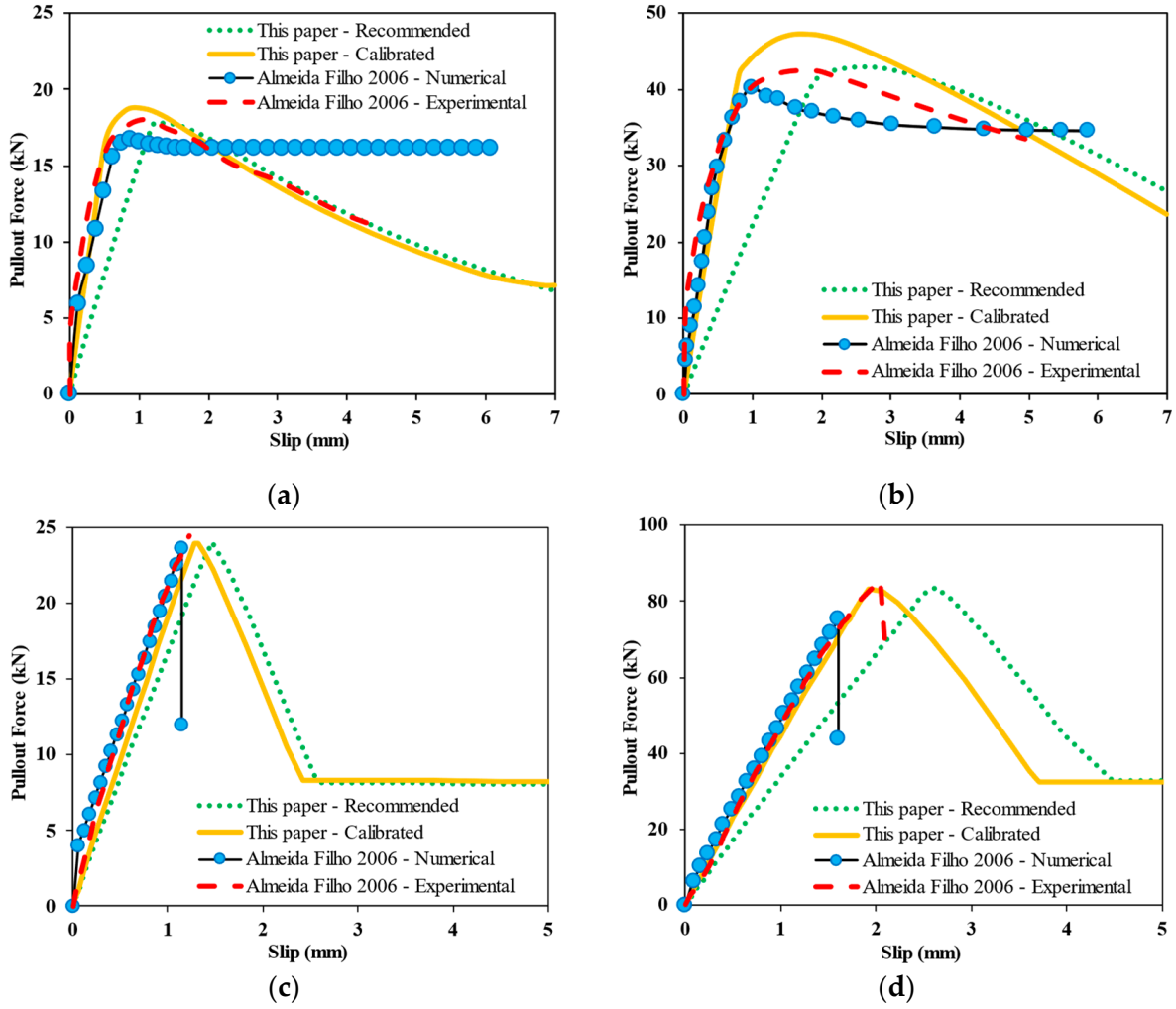


Figure 7. Analysis results for the pullout models [20]: (**a**) A-C30-B10; (**b**) A-C30-B16; (**c**) A-C60-B10; (**d**) A-C60-B16.

Table 4. Pullout models cohesive parameters.

Specimen	K_{nn} (MPa/mm)		$K_{ss} = K_{tt}$ (MPa/mm)	
	Recommended	Fitted	Recommended	Fitted
A-C30-B10	1177	3000	11.77	30
A-C30-B16	642	2000	6.42	20
A-C60-B10	1279	1500	12.79	15
A-C60-B16	1037	1500	10.37	15

As for the numerical models developed by [20] using the Mohr-Coulomb modified model, it was observed that the results were more accurate in the simulation of specimens that ruptured due to splitting. In the others, the post-peak response did not represent the experimental result well.

Numerous attempts were made during the fitting process to establish cohesive parameters that best represent the experimental behavior of the specimens. The curve-fitted numerical models closely approximated the experimental response. While there was no significant improvement in the maximum pullout force, the fitted models showed substantial improvement in predicting slip at the ultimate load, with values closely matching the experimental data.

As illustrated in Figure 7, except for the A-C30-B16 model, the differences between the pullout forces of experimental results and the fitted numerical models were less than 5%. The A-C30-B16 model exhibited a variation of around 15%, though its maximum slip value was very close to the experimental value. Additionally, Figure 7b,d shows that the reference numerical models using the modified Mohr-Coulomb model and 16 mm bars predicted lower slips than the tests, although they accurately reproduced the ultimate load of each specimen. This discrepancy may be due to mesh refinement for these models with larger diameter bars. In general, the pullout models using Equations (2) and (3) to estimate the cohesive parameters produced results lower than expected when compared to the experiments. For these models, the fitting process was essential for achieving a more accurate numerical response.

Figure 8 presents an accuracy evaluation of the developed numerical models against the numerical models by the referenced author, considering the experimental results. It is noteworthy that the experimental results are represented exactly over the equality line solely for comparison purposes with predicted results. This demonstrates that surface-based cohesive modeling with fitted parameters is capable of accurately predicting the pullout force and the maximum slip in pullout tests.

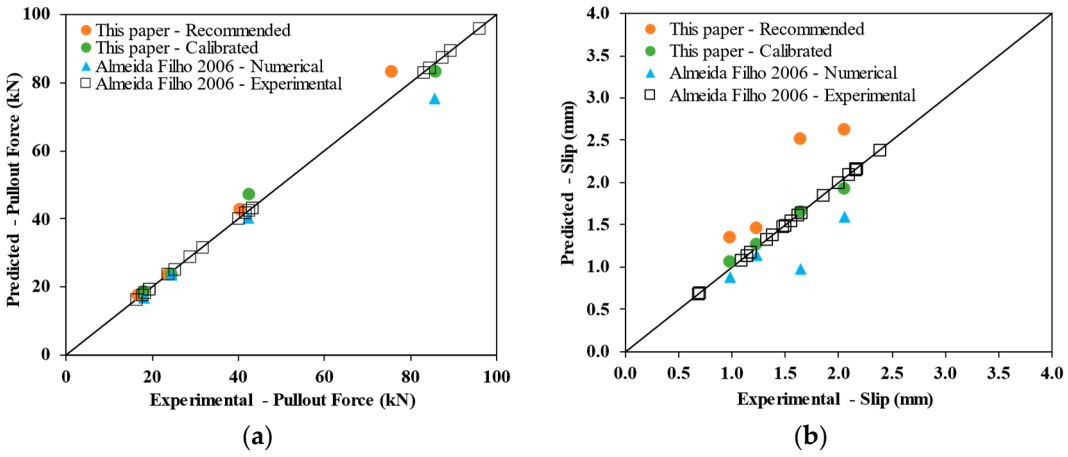


Figure 8. Accuracy evaluation of the pullout models [20]: (**a**) pullout force; (**b**) slip at the maximum pullout force.

Figure 9 shows an evaluation of the models with the same steel bar that had a variation in the compressive strength of concrete from 30 MPa to 60 MPa. Reductions of approximately 88% and 66% were observed in the differences between the fitted and recommended values for the tangential cohesive parameters (K_{ss} and K_{tt}) when this increase occurred between the models with bars of 10 mm and 16 mm, respectively.

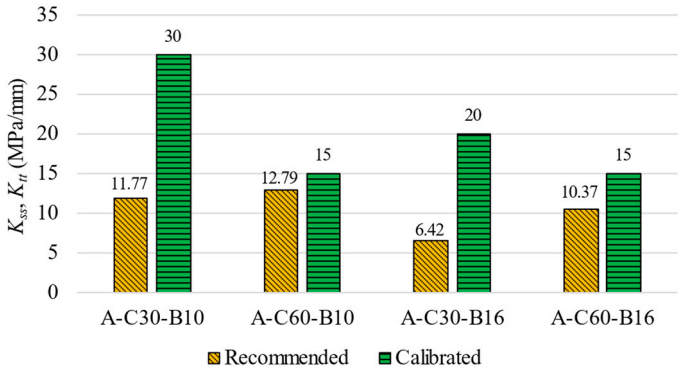


Figure 9. Differences between fitted and recommended tangential cohesive parameters ($K_{nn,}$ K_{tt}) when varying the concrete compressive strength (f_{cm}).

The behavior observed in Figure 9 showed that it may be related to the specimens' failure mode, where the models with 60 MPa concrete showed a sudden failure after the maximum pullout force, while the models with 30 MPa concrete showed softening after the ultimate load. Therefore, the recommended values better approximate the experimental behavior when the failure mode is abrupt after the ultimate load, which can happen the more resistant the concrete is.

Regarding pullout loads, it was observed that the variation in the rebar diameter caused more significant increases than the concrete compressive strength variation, as shown in Table 5. The proposed models were able to also capture those variations. It is observed an underprediction of this variation for concrete strength and the thicker bar (16 mm).

Table 5. Increases in pullout loads due to variations in bar diameter and concrete compressive strength.

Constant	Variation	Experimental Results [11] (%)	This Paper—Fitted (%)
C30 (f_{cm})	B10 to B16 (ø)	+134	+152
C60 (f_{cm})	B10 to B16 (ø)	+251	+248
B10 (ø)	C30 to C60 (f_{cm})	+35	+28
B16 (ø)	C30 to C60 (f_{cm})	+102	+76

4.2. Beam Model

Regarding the beam models, the experimental results were compared in terms of load deflection in the mid-span and load–slip of the steel bar used in the test. Only C30 concrete-grade experimental tests had the bar slip data successfully obtained. For this reason, only the load-deflection curves are presented for specimens with 60 MPa concrete.

The numerical simulation of this test with the literature-recommended cohesive parameters showed satisfactory results for all models, except for specimen V-C60-B10. In this sample, the bar slip value was very small at contact failure, thus leading to a very high value for the cohesive parameters K_{nn} and K_{tt}, as seen in Table 2. Thus, the parameters were fitted to better represent the experimental behavior. Figure 10 presents the post-processing results obtained for the computational model V-C30-B10. It observed the maximum tensile stresses in the interface zone between steel and concrete, reaching the concrete tensile strength and starting contact failure.

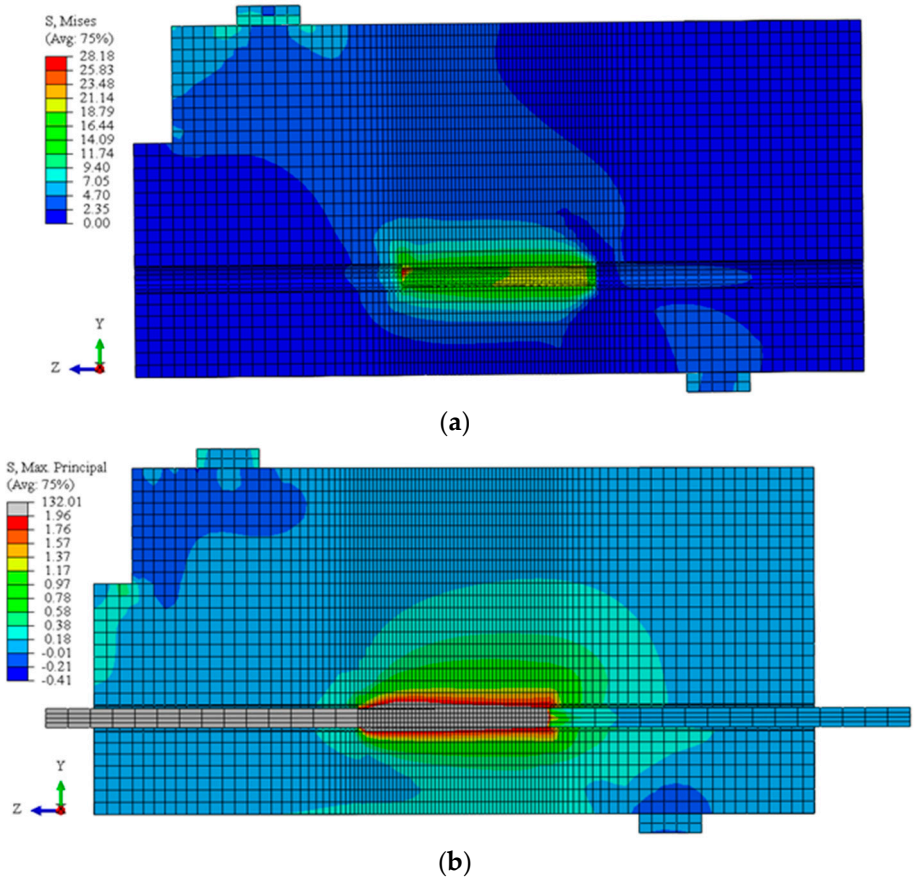


Figure 10. Stresses at the final of pullout simulation of V-C30-B10 model: (**a**) Von Mises; (**b**) Maximum Principal.

Figures 11 and 12 present the V-C30-B10 and V-C30-B16 results, respectively. The load-displacement curve for the two models with 60 MPa concrete, including fitting performed on the V-C60-B10 model, is shown in Figure 13. The displacement control used in the numerical analyses produces sudden load drops after the ultimate load, differing from the experimental test and the other reference numerical models, which used load control.

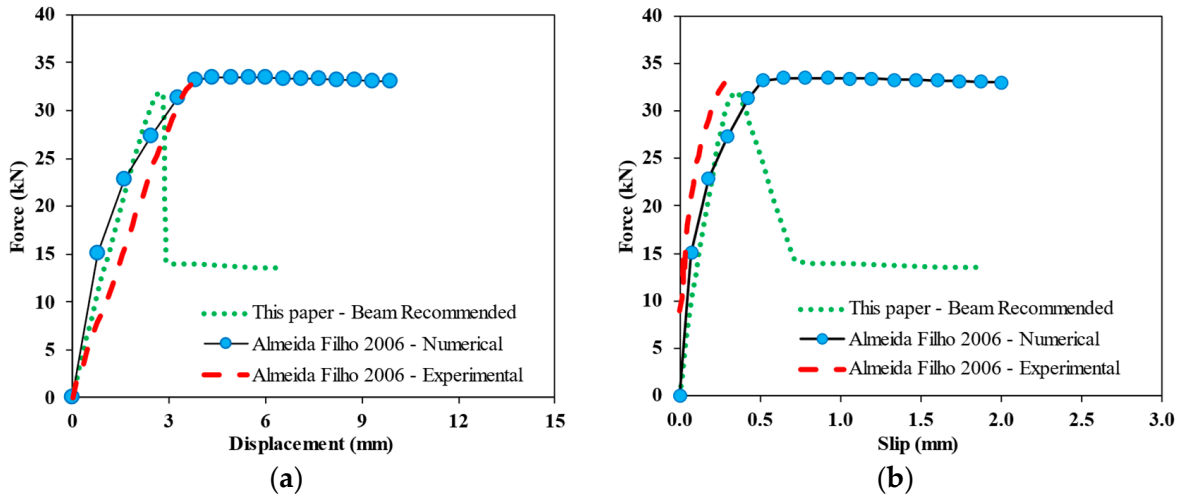


Figure 11. V-C30-B10 results [20]: (**a**) force-displacement; (**b**) force–slip.

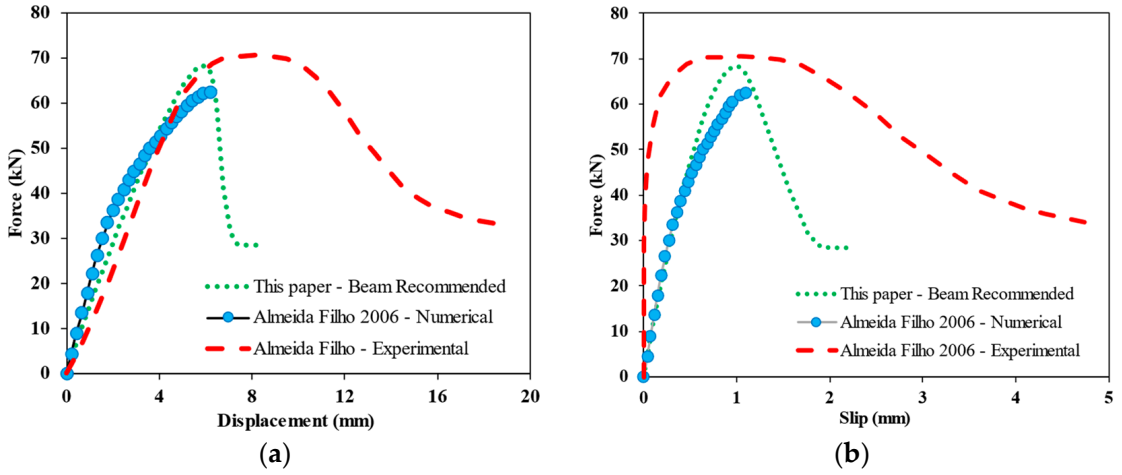


Figure 12. V-C30-B16 results [20]: (**a**) force-displacement; (**b**) force–slip.

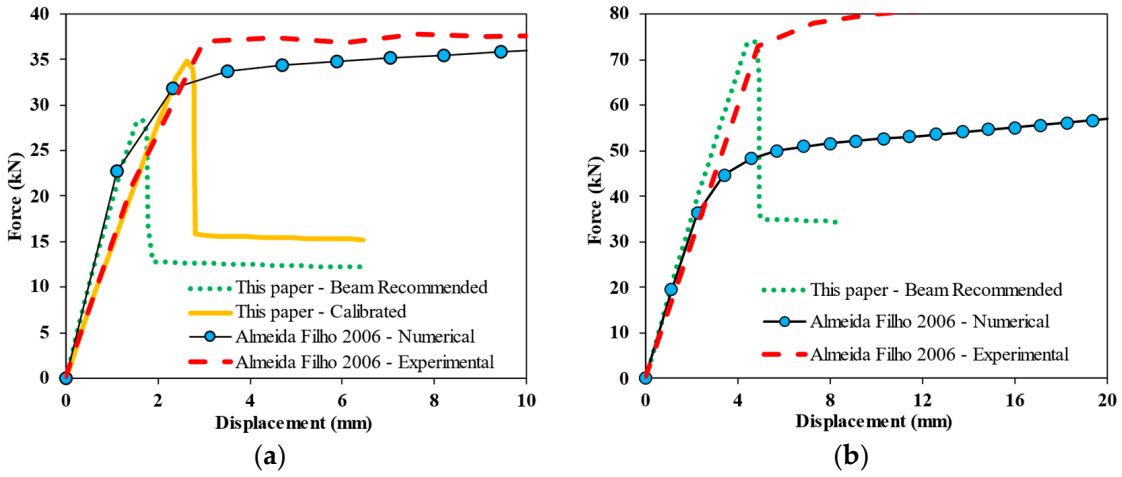


Figure 13. V-C60 force-displacement results [20]: (**a**) V-C60-B10; (**b**) V-C60-B16.

The high recommended value for the tangential component of the V-C60-B10 model shown in Figure 13a, equal to 243.38, did not produce a satisfactory result. Both the load and the beam deflection measure were underpredicted by the numerical model. Based on the recommended values for the experimental data of the beam test, the parameter fitting updated the values of the normal and tangential components to 5000 and 50 MPa/mm, respectively. With these new values, the numerical model was very close to the experimental one, improving the ultimate load and beam deflection predictions at this point.

Generally, the surface-based cohesive modeling of the steel-concrete contact interaction simulates the experimental behavior of the beam tests. The use of symmetry in three-dimensional modeling, especially in this case in which the steel bar was modeled with solid elements, made it easier to position the parts and understand the stress field formed by the relative sliding between the steel bar and the concrete.

Again, the experimental results are represented exactly over the equality line only for comparison purposes with predicted results. The results presented in Figure 14 consider the cohesive parameters recommended according to the literature for beam tests applied to all models, except for model V-C60-B10, which used fitted parameters.

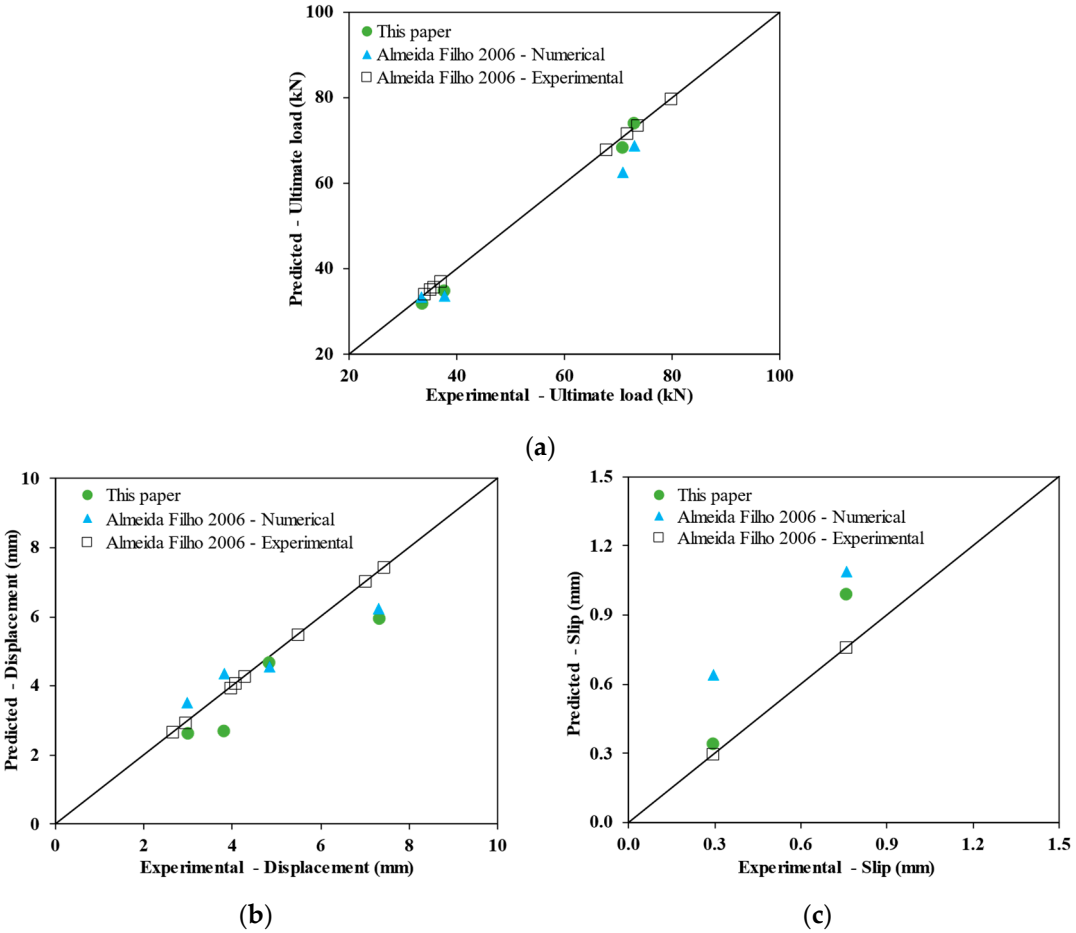


Figure 14. Accuracy evaluation of the beam models [20]: (**a**) ultimate load; (**b**) displacement at the beam mid-span; (**c**) slip.

In the beam models, the recommended values for the cohesive parameters, according to [41], did not result in significant differences between the experimental and numerical results, especially for the ultimate load. For the displacement and slip results, adjusting the parameters improved the numerical responses.

4.3. Evaluation of Pullout Cohesive Parameters Applied in Beam Tests

Without beam tests to calculate the cohesive parameters recommended for the numerical analysis, the numerical beam model's performance was evaluated using the cohesive parameters fitted for the respective pullout tests. Considering the similarities in the concrete compressive strength and the diameter of the steel bar used in the pullout test, the fitted parameters of the models with the same characteristics were applied to evaluate the impact caused on the numerical responses. Table 6 presents the beam model cohesive parameters and the pullout model fitted parameters, which were applied to the beam models.

Table 6. Cohesive parameters evaluation.

Specimen	Beam Models		Specimen	Pullout Models	
	K_{nn} (MPa/mm)	$K_{ss} = K_{tt}$ (MPa/mm)		K_{nn} (MPa/mm)	$K_{ss} = K_{tt}$ (MPa/mm)
V-C30-B10	4519	45.19	A-C30-B10	3000	30
V-C30-B16	1741	17.41	A-C30-B16	2000	20
V-C60-B10	5000	50.00	A-C60-B10	1500	15
V-C60-B16	2568	25.68	A-C60-B16	1500	15

Figure 15 presents the comparison of the results obtained with the recommended values according to the experimental beam test and with the fitted values obtained through the pullout test for the same type of concrete and the same diameter of the pulled bar. Regarding the ultimate load, there was an underprediction of 0.8%, and regarding slippage, an overprediction of about 14%.

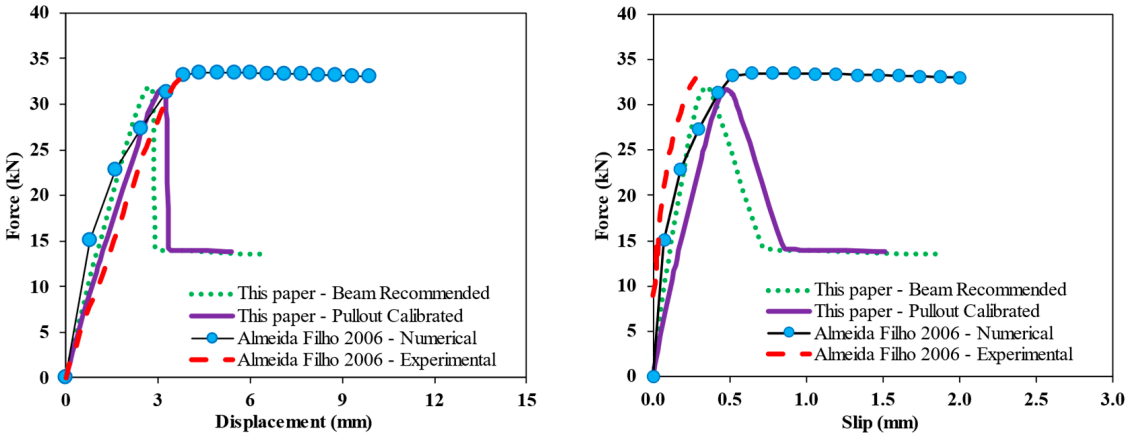


Figure 15. V-C30-B10 test with pullout fitted cohesive parameters [20]: (**a**) force-displacement; (**b**) force–slip.

Regarding the force-displacement curve, the use of fitted parameters for the pullout model produced an approximation of the numerical response to the experimental curve. On the other hand, in the force-slip curve, the parameters deviated from the numerical answer from the experimental curve, increasing the slip in the ultimate load.

In the same manner, Figure 16 presents the results obtained for the V-C30-B16 model. In this case, an even smaller difference of 0.1% in the ultimate load was observed, while for the slip measurement, there was a reduction of approximately 7%.

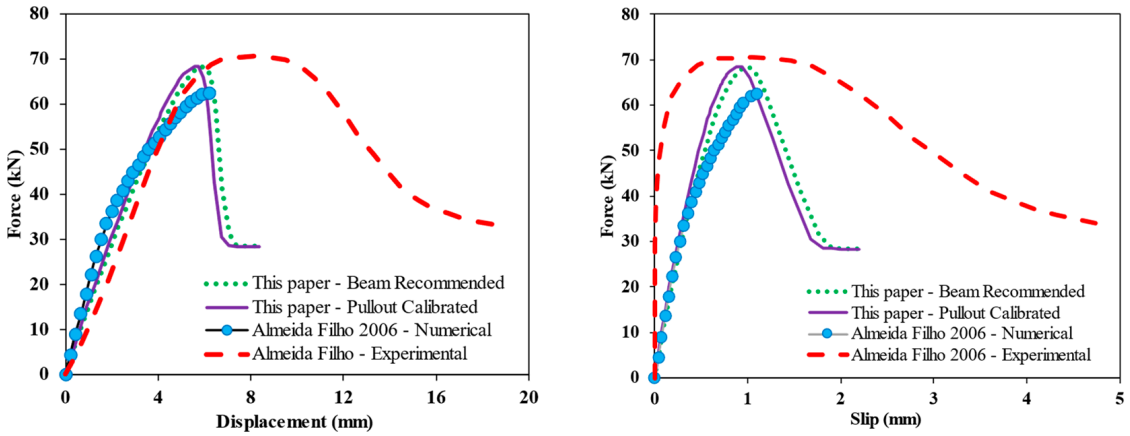


Figure 16. V-C30-B16 test with pullout fitted cohesive parameters [20]: (**a**) force-displacement; (**b**) force–slip.

The results for the last two models with 60 MPa concrete are presented in Figure 17. In the V-C60-B10 model, there was a small increase of about 3% in the ultimate load and a significant increase of 49% in the deflection value. As for the V-C60-B16 model, an increase

of 7.6% was observed in the estimate of the ultimate load, while there was an increase of about 25% in the beam deflection at the moment of maximum load.

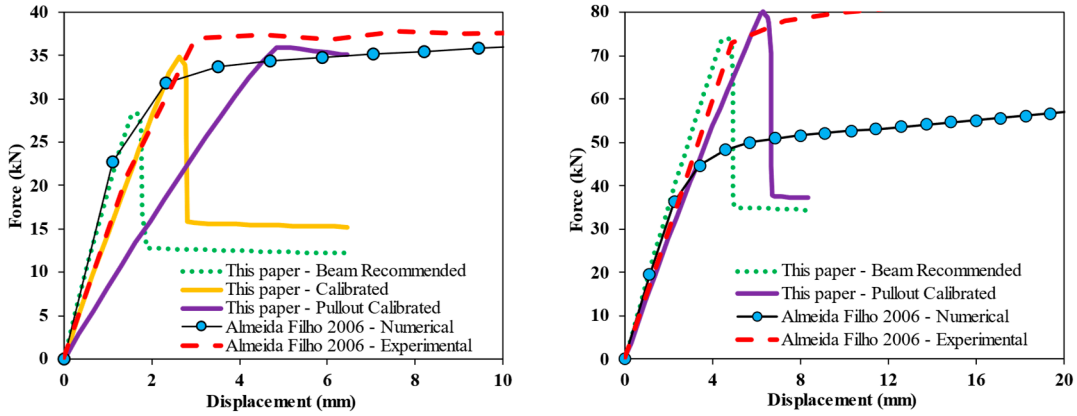


Figure 17. V-C60 tests with pullout fitted cohesive parameters [20]: (**a**) V-C60-B10; (**b**) V-C60-B16.

In the same way as the accuracy checks for the recommended and fitted values for the beam models, Figure 18 presents the comparison between the fitted values of the pullout models when applied to the beam models. It is confirmed that, regarding the ultimate load, the predictions are not significantly altered, but the other responses are affected. The beam deflection results were better predicted with the beam model parameters. On the other hand, the bar slipping results were better predicted with the parameters of the pullout models.

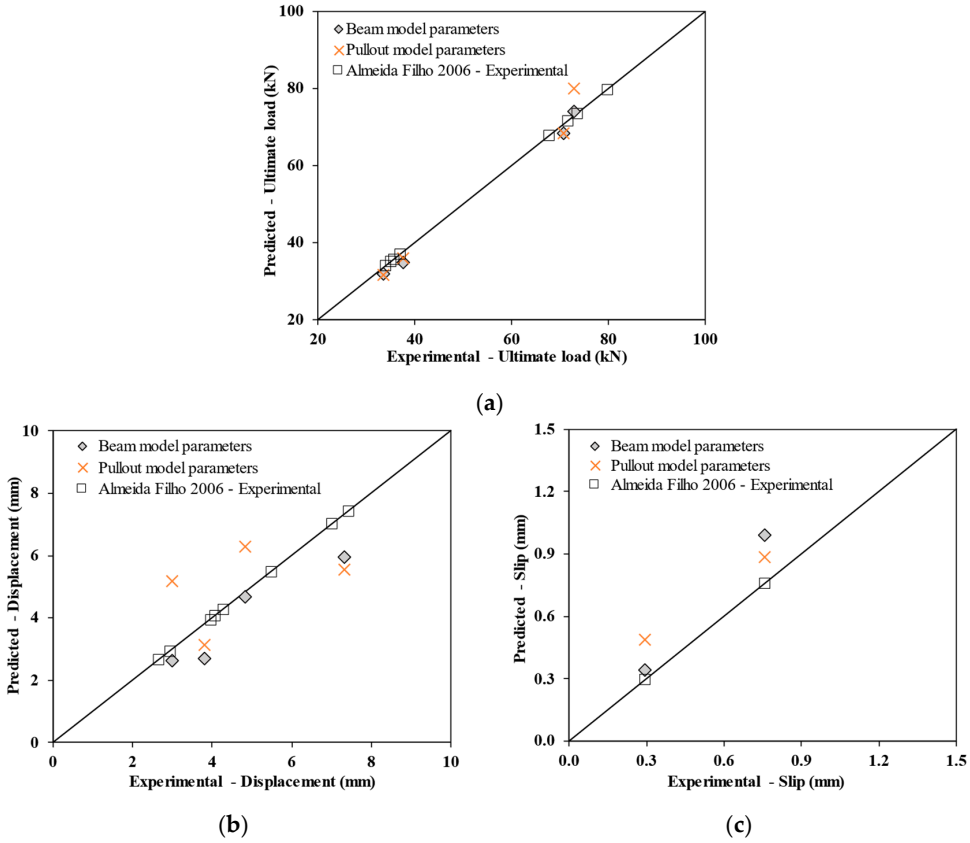


Figure 18. Accuracy evaluation of the pullout fitted parameters in the beam models [20]: (**a**) ultimate load; (**b**) displacement at the beam mid-span; (**c**) slip.

5. Conclusions

The surface-based modeling technique was employed to represent the contact interaction between steel and concrete. Numerical–experimental research from the literature on pullout and beam tests served as a reference for fitting the cohesive parameters of the developed models. Comparisons with other studies that simulated similar experiments using the same techniques were limited due to the availability of detailed modeling information, such as properties of the constitutive models, damage parameters, and surface interaction properties. Therefore, the numerical results of this study were validated against experimental test results, which proved sufficient to draw the research conclusions.

In general, the three-dimensional computational models accurately simulated the behavior of the experimental pullout tests, particularly after the cohesive parameters fitting process. The surface-based technique proved efficient, easy to model in the computational tool, and produced good results compared to other numerical studies and experimental tests. For the pullout models, the cohesive parameters fitting process yielded better results than those obtained with the recommended values. Improvements were especially significant regarding slippage at the maximum pullout force and the similarity between the load–slip curves of the numerical model and the experimental test. No significant differences were observed in the maximum pullout force between the fitted and recommended values, although numerically, all fitted values were higher. When the concrete compressive strength increased from 30 MPa to 60 MPa, significant reductions of 88% and 66% were observed in the differences between the fitted and recommended values. For the beam models, all recommended values for the cohesive parameters produced satisfactory results compared to experimental results, except for the V-C60-B10 model. The fitting process for this exception model was necessary due to the low experimental slip value at the maximum pullout force, resulting in a very high recommended cohesive parameter, which was considered an outlier.

Overall, the use of pullout test-fitted parameters in the beam models had a smaller influence on the ultimate load predictions (0.8% of the difference). However, the slippage predictions and beam deflection at the ultimate load were more affected by the change in cohesive parameters, with about a 14% difference. Although the adjusted cohesive parameters do not present a unique solution as they are obtained through several variables in non-linear problems, accuracy was achieved through error minimization based on the numerical response and the physical sense of the value intervals for each parameter. Thus, obtaining good results regarding the ultimate load without the need for beam tests, which are more expensive and complex than pullout tests, is considered an advantage. The trends observed in this paper were limited to fewer material properties, such as concrete grade, specimen size, and rebar diameter. To expand and generalize the conclusions, a broader analysis must be conducted, investigating other material properties and test configurations.

Author Contributions: Conceptualization, F.E.J., M.H.O., and P.F.M.S.; methodology, F.E.J. and P.F.M.S.; software, P.F.M.S.; validation, P.F.M.S.; formal analysis, P.F.M.S.; investigation, P.F.M.S.; resources, F.E.J. and M.H.O.; data curation, P.F.M.S.; writing—original draft preparation, P.F.M.S.; writing—review and editing, P.F.M.S., F.E.J., and M.H.O.; visualization, P.F.M.S.; supervision, F.E.J.; project administration, F.E.J.; funding acquisition, F.E.J. and M.H.O. All authors have read and agreed to the published version of the manuscript.

Funding: This work was carried out with the support of the Coordination for the Improvement of Higher Education Personnel (CAPES), the National Council for Scientific and Technological Development (CNPq), and the Federal District Research Support Foundation (FAPDF) from Brazil.

Data Availability Statement: The authors confirm that the data supporting the findings of this study are available within the article.

Acknowledgments: The authors would like to thank the organizations who provided financial support for this research, including the Coordination for the Improvement of Higher Education Personnel (CAPES), the National Council for Scientific and Technological Development (CNPq), and the Federal District Research Support Foundation (FAPDF).

Conflicts of Interest: The authors declare no conflicts of interest.

References

1. Wolenski, A.R.V.; De Castro, S.S.; Penna, S.S.; Pitangueira, R.L.S.; Silva, B.V.; Barbosa, M.P. Experimental and finite element analysis of bond-slip in reinforced concrete. *Rev. IBRACON Estrut. Mater.* **2015**, *8*, 787–799. [CrossRef]
2. Yeih, W.; Huang, R.; Chang, J.J.; Yang, C.C. A pullout test for determining interface properties between rebar and concrete. *Adv. Cem. Bas. Mat.* **1997**, *5*, 57–65. [CrossRef]
3. Kwak, H.-G.; Kim, S.-P. Bond-slip behavior under monotonic uniaxial loads. *Eng. Struct.* **2001**, *23*, 298–309. [CrossRef]
4. Almeida Filho, F.M.; Nardin, S.; El Debs, A.L.H.C. Numerical approach of the steel-concrete bond behavior using pull-out models. *Matéria* **2019**, *24*, 12341. [CrossRef]
5. Almeida Filho, F.M.; El Debs, M.K.; El Debs, A.L.H.C. Numerical approach of the bond behavior of steel bars embedded in self-compacting concrete and in ordinary concrete using beam models. *Rev. IBRACON Estrut. Mater.* **2013**, *6*, 499–512. [CrossRef]
6. Bond of reinforcement in concrete, State-of-art report fib bulletin 10. In *Fédération Internationale du Béton*; International Federation for Structural Concrete (fib): Lausanne, Switzerland, 2000.
7. Tavares, A.J.; Barbosa, M.P.; Bittencourt, T.N.; Lorrain, M. Bond steel-concrete: Simulation analysis of the pull-out tests and APULOT using the program ATENA. *Rev. IBRACON Estrut. Mater.* **2014**, *7*, 138–157. [CrossRef]
8. Pereira, H.F.S.G.; Cunha, V.M.C.F.; Sena-Cruz, J. Numerical simulation of galvanized rebars pullout. *Frat. Ed Int. Strut.* **2015**, *31*, 54–66. [CrossRef]
9. Hassoun, M.N.; Al-Manaseer, A. *Structural Concrete: Theory and Design*, 6th ed.; Wiley: Hoboken, NJ, USA, 2015.
10. Dugdale, D.S. Yielding of steel sheets containing slits. *J. Mech. Phys. Solids* **1960**, *8*, 100–104. [CrossRef]
11. Barenblatt, G.I. The mathematical theory of equilibrium cracks in brittle fracture. *Adv. Appl. Mech.* **1962**, *7*, 55–129. [CrossRef]
12. Evangelista, F., Jr.; Roesler, J.; Paulino, G.H. Numerical simulations of fracture resistance of functionally graded concrete materials. *Transp. Res. Rec.* **2009**, *2113*, 122–131. [CrossRef]
13. Evangelista, F., Jr.; Roesler, J.; Proença, S.P. Three-dimensional cohesive zone model for fracture of cementitious materials based on the thermodynamics of irreversible processes. *Eng. Fract. Mech.* **2013**, *97*, 261–280. [CrossRef]
14. Park, K.; Paulino, G.H. Cohesive zone models: A critical review of traction-separation relationships across fracture surfaces. *Appl. Mech. Rev.* **2011**, *64*, 06802. [CrossRef]
15. Reda, R.; Omar, Z.; Sallam, H.; Ahmad, S.S.E. Effect of different parameters controlling the flexural behavior of RC beams strengthened with NSM using nonlinear finite element analysis. *Frat. Integ. Strut.* **2020**, *53*, 106–123. [CrossRef]
16. Abbas, M.; Bary, B.; Jason, L. A 3D mesoscopic frictional cohesive zone model for the steel-concrete interface. *Int. J. Mech. Sci.* **2023**, *237*, 107819. [CrossRef]
17. Abbas, M.; Bary, B.; Jason, L. 3D mesoscale analysis of the effects of steel bar ribs geometry on reinforced concrete bond strength. *Fin. Elem. Anal. Des.* **2023**, *219*, 103928. [CrossRef]
18. Burdziński, M.; Niedostatkiewicz, M. Experimental-Numerical Analysis of the Effect of Bar Diameter on Bond in Pull-Out Test. *Buildings* **2022**, *12*, 1392. [CrossRef]
19. Rolland, A.; Argoul, P.; Benzarti, K.; Quiertant, M.; Chataigner, S.; Khadour, A. Analytical and numerical modeling of the bond behavior between FRP reinforcing bars and concrete. *Constr. Build. Mater.* **2020**, *231*, 117160. [CrossRef]
20. Almeida Filho, F.M. Contribution to the Study of Bond Slip between Steel Bars and Self-Compacting Concrete. Ph.D. Thesis, Departamento de Engenharia de Estruturas da Escola de Engenharia de São Carlos da Universidade de São Paulo (SET/EESC/USP), São Carlos, SP, Brazil, 2006. (In Portuguese).
21. Rilem, T.C. RC 6 Bond test for reinforcement steel. 2. Pull-out test. In *RILEM Technical Recommendations for the Testing and Use of Construction Materials*; CRC Press: Boca Raton, FL, USA, 1994; pp. 218–220. [CrossRef]
22. Rilem, T.C. RC 5 Bond test for reinforcement steel. 1. Beam test. In *RILEM Technical Recommendations for the Testing and Use of Construction Materials*; CRC Press: Boca Raton, FL, USA, 1994; pp. 213–217. [CrossRef]
23. Huang, Y.; Liu, Y. Review of Bond-Slip Behavior between Rebar and UHPC: Analysis of the Proposed Models. *Buildings* **2023**, *13*, 1270. [CrossRef]
24. Gujar, A.; Pore, S.; Prakash, V. Modeling in ABAQUS for experimental investigation of multi-linear bond slip properties in reinforced concrete. *Int. J. Adv. Eng. Res. Develop.* **2008**, *6*, 155–163.
25. Khalfallah, S. Modeling of bond for pull-out tests. *Build. Res. J.* **2008**, *56*, 37–48.
26. Senthil, K.; Bawa, S.; Aswin, C.P. Influence of concrete strength and diameter of reinforcing bar on pullout tests using finite element analysis. *J. Struct. Eng. Appl. Mec.* **2018**, *1*, 105–116. [CrossRef]
27. Dassault Systèmes Simulia Corp. *Abaqus User's Manual*; Dassault Systèmes Simulia Corp: Providence, RI, USA, 2017.
28. Salve, A.K.; Jalwadi, S.N. Implementation of Cohesive Zone in ABAQUS to Investigate Fracture Problems. National Conference for Engineering Post Graduate RIT. May 2015. Available online: https://www.researchgate.net/publication/310774819 (accessed on 29 June 2024).
29. Bravo, M.; Duarte, A.P.C.; de Brito, J.; Evangelista, L. Tests and simulation of the bond-slip between steel and concrete with recycled aggregates from CDW. *Buildings* **2021**, *11*, 40. [CrossRef]
30. Mathern, A.; Yang, J. A practical finite element modeling strategy to capture cracking and crushing behavior of reinforced concrete structures. *Materials* **2021**, *14*, 506. [CrossRef]

31. Noman, M.; Ahmad, W.; Ullah, B.; Ahmed, A. Numerical modelling of bond-slip behavior in a RC beam using ABAQUS. In Proceedings of the 1st International Conference on Recent Advances in Civil and Earthquake Engineering (ICCEE-2021), Peshawar, Pakistan, 8 October 2021.
32. Deng, N.; Zhao, H.; Yao, D.; Tang, Z. Bond-Slip Performances of Ultra-High Performance Concrete Steel Tube Columns Made of a Large-Diameter Steel Tube with Internally Welded Steel Bars. *Materials* **2023**, *16*, 3836. [CrossRef]
33. Wu, G.; Wang, H. Numerical Simulation of Steel Fiber Pull-Out Process Based on Cohesive Zone Model and Unified Phase-Field Theory. *Sustainability* **2023**, *15*, 4015. [CrossRef]
34. Sun, Z.; Feng, D.-C.; Sun, Y.; Yuan, J.; Li, X.; Wei, Y. Bond-slip behavior of bundled steel/FRP bars and its implementation in high-fidelity FE modeling of reinforced concrete beams. *Constr. Build. Mater.* **2021**, *286*, 122887. [CrossRef]
35. Wang, X.; Liu, Y.; Yang, F.; Lu, Y.; Li, X. Effect of concrete cover on the bond-slip behavior between steel section and concrete in SRC structures. *Constr. Build. Mater.* **2019**, *229*, 116855. [CrossRef]
36. Roscini, F.; Guadagnini, M. Bond Behavior of Steel Cords Embedded in Inorganic Mortars. *Materials* **2022**, *15*, 5125. [CrossRef]
37. Sun, G.; Bai, X.; Sang, S.; Zeng, L.; Yin, J.; Jing, D.; Zhang, M.; Yan, N. Numerical Simulation of Anchorage Performance of GFRP Bolt and Concrete. *Buildings* **2023**, *13*, 493. [CrossRef]
38. German, M.; Pamin, J. Cracking in Reinforced Concrete Cross-Sections Due to Non-Uniformly Distributed Corrosion. *Materials* **2023**, *16*, 6331. [CrossRef]
39. Brisotto, D.S.; Bittencourt, E.; d'A Bessa, V.M.R. Simulating bond failure in reinforced concrete by a plasticity model. *Comput. Struct.* **2012**, *106–107*, 81–90. [CrossRef]
40. Beliaev, M.; Semenov, A.; Semenov, S.; Benin, A. Simulation of pulling the reinforcing bar from concrete block with account of friction and concrete damage. *MATEC Web Conf.* **2016**, *73*, 04010. [CrossRef]
41. Luna Molina, F.J.; Fernández Ruiz, M.A.; Hernández Montes, E.; Alonso Alonso, M.C. Bond strength of galvanized steel: Experimental and numerical study based on pull-out tests. In Proceedings of the 3rd International Conference on Mechanical Models in Structural Engineering, Seville, Spain, 24–26 June 2015.
42. Henriques, J.; Simões da Silva, L.; Valente, I.B. Numerical modeling of composite beam to reinforced concrete wall joints. Part I: Fitting of joints components. *Eng. Struct.* **2013**, *52*, 747–761. [CrossRef]
43. Gan, Y. Bond Stress and Slip Modeling in Nonlinear Finite Element Analysis of Reinforced Concrete Structures. Master's Thesis, University of Toronto, Toronto, ON, Canada, 2000.
44. Keuser, M.; Mehlhorn, G.; Cornelius, V. Bond between Prestressed Steel and Concrete—Computer Analysis Using ADINA. *Comput. Struct.* **1983**, *17*, 669–676.
45. fib Model Code 2010: For concrete structures. In *Fédération Internationale du Béton*; Wilhelm Ernst & Sohn: Berlin, Germany, 2013; ISBN 978-3-433-03061-5.
46. Lundgren, K. Bond between ribbed bars and concrete. Part 1: Modified model. *Mag. Conc. Res.* **2005**, *57*, 371–382. [CrossRef]
47. Alfarah, B.; López-Almansa, F.; Oller, S. New methodology for calculating damage variables evolution in Plastic Damage Model for RC structures. *Eng. Struct.* **2017**, *132*, 70–86. [CrossRef]
48. Vermeer, P.A.; De Borst, R. Non-associated plasticity for soils, concrete and rock. *Heron* **1984**, *29*, 5–16.
49. Bezerra, L.M.; Barbosa, W.C.S.; Bonilla, J.; Cavalcante, O.R.O. Truss-type shear connector for composite steel-concrete beams. *Constr. Build. Mater.* **2018**, *167*, 757–767. [CrossRef]
50. Bezerra, L.M.; Cavalcante, O.R.O.; Chater, L.; Bonilla, J. V-shaped shear connector for composite steel-concrete beam. *J. Constr. Steel Res.* **2018**, *150*, 162–174. [CrossRef]
51. Lima, J.M.; Bezerra, L.M.; Bonilla, J.; Silva, R.S.Y.R.C.; Barbosa, W.C.S. Behavior and resistance of truss-type shear connector for composite steel-concrete beams. *Steel Comp. Struct.* **2020**, *36*, 569–586. [CrossRef]
52. Lima, J.M.; Bezerra, L.M.; Bonilla, J.; Barbosa, W.C.S. Study of the behavior and resistance of right-angle truss shear connector for composite steel concrete beams. *Eng. Struct.* **2022**, *253*, 113778. [CrossRef]
53. Mirhosseini, R.T.; Araghizadeh, E.; Rashidi, S. Approximate Relationship for the Bond-Slip Using a Concrete Damage-Plastic Model. *Adv. Mat. Sci. Eng.* **2023**, *2023*, 1320192. [CrossRef]
54. Araghizadeh, E.; Mirhosseini, R.T.; Rashidi, S.; Nejad, M.N. Investigation of bond-slip in reinforced steel rebar using concrete damage-plastic model. *Innov. Infr. Solut.* **2023**, *8*, 37. [CrossRef]
55. Santana, P.F.M.; Silva, P.C.S.; Ferreira, M.P.; Bezerra, L.M.; Oliveira, M.H. Experimental and numerical study of headed bars embedded in RC members under tension. *Int. J.* **2022**, *84*, 531–546. [CrossRef]
56. Evangelista, F., Jr.; Alves, G.S.; Moreira, J.F.A.; Paiva, G.O.F. A global-local strategy with the generalized finite element framework for continuum damage models. *Comput. Methods Appl. Mech. Eng.* **2020**, *363*, 112888. [CrossRef]
57. Evangelista, F., Jr.; Moreira, J.F.A. A novel continuum damage model to simulate quasi-brittle failure in mode I and mixed-mode conditions using a continuous or a continuous-discontinuous strategy. *Theor. Appl. Fract. Mech.* **2020**, *109*, 102745. [CrossRef]

58. Lima, J.P.S.; Evangelista, F., Jr.; Soares, C.G. Hyperparameter-optimized multi-fidelity deep neural network model associated with subset simulation for structural reliability analysis. *Reliab. Eng. Syst. Saf.* **2023**, *239*, 109492. [CrossRef]
59. Lima, J.P.S.; Evangelista, F., Jr.; Soares, C.G. Bi-fidelity Kriging model for reliability analysis of the ultimate strength of stiffened panels. *Mar. Struct.* **2023**, *91*, 103464. [CrossRef]

Disclaimer/Publisher's Note: The statements, opinions and data contained in all publications are solely those of the individual author(s) and contributor(s) and not of MDPI and/or the editor(s). MDPI and/or the editor(s) disclaim responsibility for any injury to people or property resulting from any ideas, methods, instructions or products referred to in the content.